THE ASTROPHYSICAL JOURNAL, 531:L9–L12, 2000 March 1

A *CHANDRA* HIGH-RESOLUTION X-RAY IMAGE OF CENTAURUS A

R. P. KRAFT, W. FORMAN, C. JONES, A. T. KENTER, S. S. MURRAY, T. L. ALDCROFT, M. S. ELVIS,
I. N. EVANS, G. FABBIANO, T. ISOBE, D. JERIUS, M. KAROVSKA, D.-W. KIM,
A. H. PRESTWICH, F. A. PRIMINI, AND D. A. SCHWARTZ
Harvard-Smithsonian Center for Astrophysics, 60 Garden Street,
Cambridge, MA 02138; rkraft@cfa.harvard.edu
E. J. SCHREIER
Space Telescope Science Institute, 3700 San Martin Drive, Baltimore, MD 21218
AND
A. A. VIKHLININ
Space Research Institute, Profsouznaya 84/32, Moscow 117810, Russia
Received 1999 November 19; accepted 2000 January 11; published 2000 February 4

ABSTRACT

We present first results from a *Chandra X-Ray Observatory* observation of the radio galaxy Centaurus A with the High-Resolution Camera. All previously reported major sources of X-ray emission including the bright nucleus, the jet, individual point sources, and diffuse emission are resolved or detected. The spatial resolution of this observation is better than 1″ in the center of the field of view and allows us to resolve X-ray features of this galaxy not previously seen. In particular, we resolve individual knots of emission in the inner jet and diffuse emission between the knots. All of the knots are diffuse at the 1″ level, and several exhibit complex spatial structure. We find the nucleus to be extended by a few tenths of an arcsecond. Our image also suggests the presence of an X-ray counterjet. Weak X-ray emission from the southwest radio lobe is also seen, and we detect 63 pointlike galactic sources (probably X-ray binaries and supernova remnants) above a luminosity limit of $\sim 1.7 \times 10^{37}$ ergs s^{-1}.

Subject headings: galaxies: active — galaxies: individual (Centaurus A, NGC 5128) — galaxies: jets — X-rays: galaxies

1. INTRODUCTION

The radio galaxy Centaurus A (NGC 5128) is the nearest active galaxy (~3.5 Mpc) and has been well studied at all wavelengths because of its proximity and complex structure over a wide range of spatial scales. Cen A is considered to be the prototype low-luminosity Fanaroff-Riley class I radio galaxy (Israel 1998). Radio maps show a strong, well-collimated jet extending ~6′ from the nucleus and a weak counterjet ~30 mas in the opposite direction (Jones et al. 1996). The jets open into bright radio lobes (the inner lobes) several arcminutes from the nucleus (Burns, Feigelson, & Schreier 1983). The giant outer lobes extend several degrees. Optically Cen A appears as an elliptical galaxy with a dark dust lane through the center. The dust lane is thought to be a thin, warped disk contained within the elliptical galaxy and may be the result of at least one merger (Schiminovich et al. 1994). Bright optical emission aligned with the jet has been reported (Brodie, Konigl, & Bowyer 1983), but *Hubble Space Telescope* (*HST*) observations reveal no emission at the locations of the radio/X-ray knots (Marconi et al. 2000). *HST* observations in the infrared have shown the presence of an extended disk 20 pc in radius around the nucleus (Schreier et al. 1998).

Previous X-ray observations of Cen A have revealed several sources of X-ray emission including a bright nucleus, a one-sided X-ray jet, complex diffuse emission, and numerous point sources (Schreier et al. 1979; Feigelson et al. 1981; Döbereiner et al. 1996; Turner et al. 1997). At the resolution (~few arcseconds) of *ROSAT* and *Einstein* HRI observations, the nucleus is consistent with a point source. The X-ray jet morphology is strikingly similar to that seen in the radio. The well-collimated X-ray jet extends about 4′ from the nucleus, and generally the position of the X-ray knots is identical to that of the radio knots. The diffuse X-ray emission from Cen A has several distinct components including weak emission from the region around both radio lobes and a general galactic component within about 6′ from the nucleus that is probably generated by main-sequence stars or the hot interstellar medium.

In this Letter, we present a high-resolution X-ray image of Cen A taken with the *Chandra X-Ray Observatory* (*CXO*; Weisskopf et al. 1995) using the High-Resolution Camera (HRC; Murray et al. 1987; Murray et al. 1997; Kenter et al. 1997; Kraft et al. 1997) as part of the orbital activation and checkout phase of the mission. The spatially complex X-ray morphology of Cen A, including the bright nucleus that dominates the flux, the diffuse jet, the point sources, and the extended diffuse emission from the galaxy and radio lobes, demonstrates the previously unprecedented imaging performance of the observatory. The goal of this Letter is to present the capabilities of the *CXO* that for the first time provides subarcsecond imaging resolution in the soft X-ray band. More detailed scientific analysis will be presented in future publications. The imaging performance of the telescope/detector combination is better than 1″ on-axis and allows us to resolve structure in the galaxy not previously seen. We have examined the nucleus for evidence of extended emission, mapped the spatial structure of the jet, and quantified the distribution of discrete sources within the galaxy to a luminosity limit of $\sim 1.7 \times 10^{37}$ ergs s^{-1}. We assume a distance of 3.5 Mpc to Cen A throughout this Letter.

2. INSTRUMENTATION AND OBSERVATIONS

The *CXO* was launched on 1999 July 23 and contains a high-resolution mirror assembly (the HRMA), two sets of focal-plane detectors, and two sets of transmission gratings for dispersive spectroscopy. A complete discussion of the satellite and

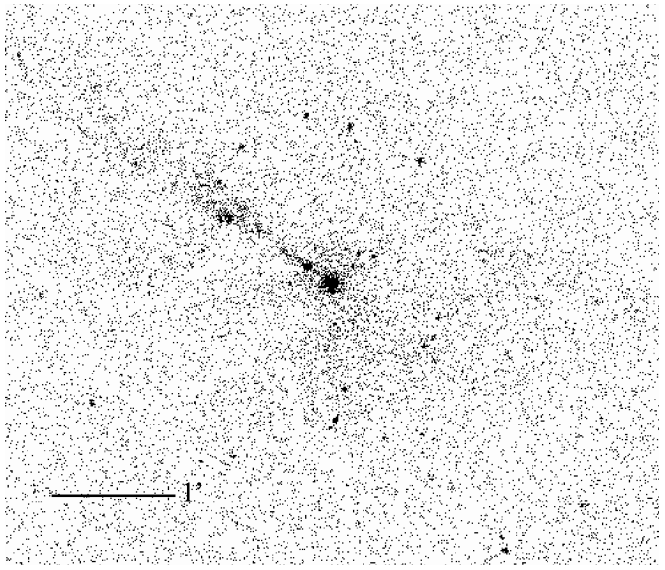

FIG. 1.—Raw X-ray image of Cen A. The nucleus is the bright source in the center of the field. North is up, and east is to the left. The bar on the image is 1′. The exposure time is 26.8 ks.

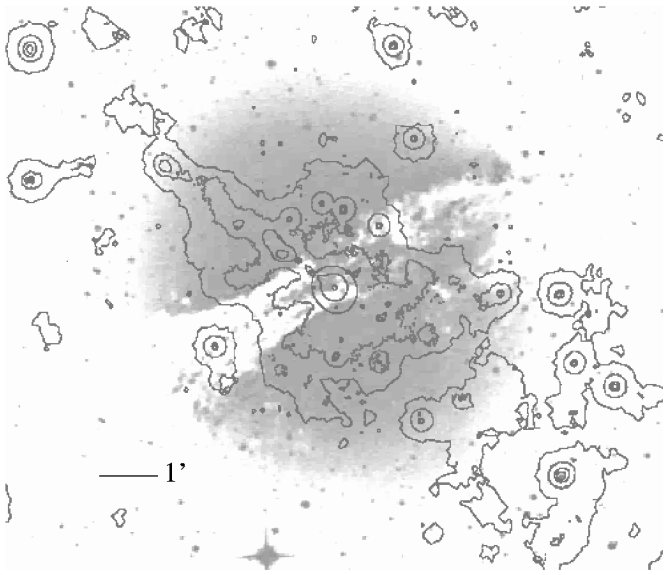

FIG. 2.—X-ray contour map overlaid on an optical Digitized Sky Survey image of Cen A. North is up, and east is to the left. The levels of the contours are 34.2, 0.259, 0.095, 0.072, and 0.054 counts arcmin^{-2} s^{-1}. The background level is 0.047 counts arcmin^{-2} s^{-1}. The three highest contours were created from a wavelet decomposition of the raw image, and the lowest two were created from an adaptive smoothing. The nucleus and inner jet can clearly be seen as well as the anticorrelation of the diffuse emission with the dust lane, emission from the southwest inner lobe, and the X-ray enhancement at the edge of the lobe.

scientific instruments is given elsewhere (Weisskopf et al. 1995 and references therein). Cen A was observed twice with the HRC imaging detector (HRC-I) on 1999 September 10 (observations 00463 and 01253). The two data sets were combined for the analysis described below. The HRC is a microchannel plate X-ray imaging detector and is a direct descendant of the *Einstein* (Giacconi et al. 1979) and *ROSAT* High-Resolution Imagers (HRIs; Zombeck et al. 1995). One pixel on the HRC is 6.43 μm, which corresponds to 0.″13175 with a total field of view of 33′ × 33′. The spatial resolution of the detector is approximately 3 pixels (FWHM). The imaging resolution of the combined HRMA + HRC is expected to be better than 1″ once the best observatory aspect solution has been applied. We used an observation of AR Lacertae, an isolated point source, as an independent measure of the point-spread function (PSF) of the combined HRMA + HRC in orbit and to estimate the significance of any image reconstruction uncertainty. We find that 90% of the power in the AR Lac observation is contained in an 2.″1 diameter circle.

There are two detector artifacts that must be addressed to achieve the best angular spatial resolution and reduce the background. The HRC uses a three tap algorithm (Murray & Chappell 1988) for event positioning. The raw event position must be corrected to account for the charge distributed beyond the three taps in each axis. This technique is called "degapping" because the raw image shows gaps halfway between each tap. Electronic noise can create small artifacts in the degapped images. From both theoretical and observational evidence, the relationship of signal on the three amplifiers is tightly constrained. It is possible therefore to identify which events have been misplaced and correct their position from this a priori knowledge of the relationship of the charge distribution among the amplifiers.

The PSF of the HRC-I detector also is contaminated by a small "ghost" image in which ~1.5% of the events are misplaced along one of the detector axes because of amplifier saturation. This ghost would, if not removed, considerably complicate the PSF and is particularly important for an observation like Cen A where we are searching for relatively weak features in the presence of a bright central source. As above, the relationship of the signal on the three amplifiers is well known, and these events can be removed because they violate this a priori condition (for details, see S. Murray et al. 2000, in preparation). This algorithm also identifies background events produced by cosmic rays that are not already vetoed by the anticoincidence shield. As a result about 45% of the raw counts are rejected, while more than 90% of the valid X-rays are accepted. As this new algorithm is tested and calibrated, it will be incorporated into HRC standard data processing.

3. DATA ANALYSIS AND RESULTS

The raw *CXO*/HRC X-ray image is shown in Figure 1. The bright nucleus can clearly be seen at the center of the image, as can the jet and many of the galactic point sources. Figure 2 contains an image of the X-ray contours of Cen A overlaid on an optical Digital Sky Survey image. The contours were created using several different smoothing algorithms to enhance the appearance of different features. The complex spatial structure of both the jet and the diffuse emission is apparent. Note that the X-ray contours in both the inner jet and diffuse regions are coincident with the regions of lower dust opacity in the optical. There is also diffuse emission to the southwest of the nucleus that may be related to the southwest inner radio lobe, as well as the previously seen (Döbereiner et al. 1996) arclike diffuse feature coincident with the edge of this radio lobe. Our analysis in this Letter focuses on the X-ray emission from the nucleus, the jet and search for a counter jet, and the discrete sources. We describe the emission from each of these in more detail below and compare with previous X-ray observations and with observations in other energy bands.

3.1. *The Nucleus*

We examined the nucleus for evidence of extent. Extended emission on ~1″ spatial scale around the nucleus has been

previously detected in both the radio (Burns et al. 1983) and the infrared (Schreier et al. 1998). We compared the encircled energy of the nuclear region of Cen A to that of an HRC observation of AR Lac and that of a raytrace simulation of the HRMA PSF at 5.5 keV smoothed by a Gaussian (σ = 2 pixels) to model the effects of image reconstruction uncertainty and the finite spatial resolution of the HRC. The reconstruction uncertainty is expected to be ~1 pixel (rms), and the spatial resolution of the HRC is 1.5 pixels (rms). The encircled energies were computed only out to 50 pixels to avoid confusion caused by other sources around the Cen A nucleus. The encircled energy curve of the nucleus of Cen A is 0.″2–0.″3 broader than the raytrace simulation, indicating that the nucleus is extended by a few tenths of an arcsecond. The encircled energies of the nucleus also are broader than that of the AR Lac observation, so that if this result is due to a larger systematic uncertainty in the image reconstruction, it must be specific to this observation. Since this measurement is at the resolution limit of the instrument, we hesitate to make a more definitive statement. The spatial extent of the nucleus is consistent with the *Einstein* HRI upper limit of ~0.″3 (Feigelson et al. 1981).

If the nucleus is extended, the origin of the diffuse emission is unclear. If 20% of the "nuclear" flux originates in hot gas within 10 pc of the nucleus, the implied density ($n \sim 10$ cm^{-3}) and therefore pressure are unrealistically large (assuming log T = 7 and 0.35 solar abundance Raymond-Smith plasma). The presence of diffuse radio and infrared emission may imply a more complex, perhaps nonthermal origin for the emission. The extended emission also could be caused by a dust-scattering halo, since we are observing the nucleus through the dust lane of the merged spiral galaxy. The optical extinction to the nucleus is only 6 mag (van den Bergh 1976), so that the large X-ray column seen in the *ROSAT* PSPC and *Einstein* IPC spectra may be local to the nucleus, although a simple computation shows the size of a dust-scattered halo would be ~0.″5 (Mauche & Gorenstein 1986). Electron scattering from ionized material local to the nucleus also may produce diffuse X-ray emission (Fabian 1977). Finally, emission from the nuclear jet is a third possibility (Burns et al. 1983).

The average count rate of the nucleus is 0.9 counts s^{-1}. Assuming a power-law spectrum with a photon index of 1.9 and a column density of 10^{23} cm^{-2} (Turner et al. 1997), the average observed flux is 1.95×10^{-10} ergs cm^{-2} s^{-1} in the 2–10 keV bandpass, yielding a luminosity of 5×10^{41} ergs s^{-1}. The count rate monotonically increased by approximately 10% over the 26.8 ks observation.

3.2. *The Jet*

A contour plot of a region 80″ × 600″ through the nucleus and jet along position angle 55°, the inner jet region, is shown in Figure 3. The contour plot was created using the small spatial scales of a wavelet decomposition. The knots in the jet are labeled as in Feigelson et al. (1981) and Burns et al. (1983). All of the X-ray knots are clearly extended. The structure of each knot can been seen in this image as well as diffuse emission between the knots at and beyond knot B. Knot B in particular has a complex morphology with at least three bright subknots. There are also several sources along a counterjet.

X-ray knot A1 in our image coincides precisely with radio knot A1 (Burns et al. 1983). In the *ROSAT* and *Einstein* data, no distinct knots of X-ray emission between A/A1 and B were observed. VLA observations indicate three additional knots of radio emission (A2, A3, and A4) between the X-ray knots A1 and B (Burns et al. 1983). We detect at least two additional

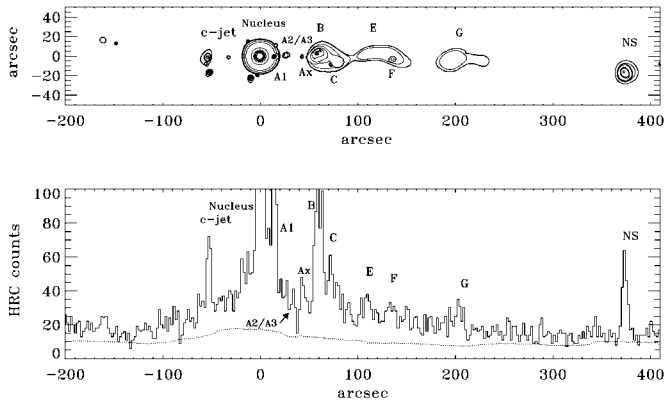

FIG. 3.—*Top:* Contour plot of the nucleus and jet of Cen A along position angle 55°. The raw data has been smoothed using the wavelet decomposition algorithm at scales 0.″5, 1″, 2″, 4″, 8″, and 16″. The lowest contour corresponds to 2.5 σ above the noise in the 16″ decomposition. *Bottom:* The histogram is the projection of a 32″ × 600″ rectangle of the raw data. The smooth curve below the histogram is an estimate of the background from regions of the image just outside the box.

knots, one between radio knots A2 and A3 (labeled A2/3 in Fig. 3), and a second with no distinct radio counterpart (labeled AX in Fig. 3). The presence of X-ray knot AX is suggested by the *ROSAT* data (Döbereiner et al. 1996), although it was not clearly separated from knot B. The region between knots A and B is crossed by the thick, irregular dust lane of the galaxy and knots A2/3 and AX correspond almost exactly with regions of lower optical extinction in the dust lane. The inner jet may emit X-rays continuously along most or all of its length from knot A1 to knot B, with the observed structure due entirely to absorption. We also detected a bright source 380″ from the nucleus beyond the northeast inner radio lobe that was not seen by *ROSAT*. The nature of this source and whether it is related to the jet is unknown.

The histogram in Figure 3 (below the contour plot) is a projection of the raw data of a region 32″ × 600″ along the same position angle. The smooth curve below the histogram is the background estimated from regions immediately above and below the region of interest. The bright source labeled c-jet, as well as extended diffuse emission along a line opposite the jet, is evident, suggesting a counterjet. Several radio knots have been detected along this line (Clarke, Burns, & Norman 1992), but we find the position of these radio knots to be displaced from the X-ray knots by several arcseconds.

We also clearly detect X-ray emission from the region of the southwest radio lobe (see Fig. 2). X-ray emission from this lobe was first reported by Morini, Anselmo, & Molteni (1989) using data taken with the *EXOSAT* Channel Multiplier Array. Other observations have suggested the presence of emission from this lobe (e.g., Turner et al. 1997), but were not able to clearly separate emission from the bright foreground star located near the outer edge of the lobe and the diffuse galactic emission from that of the lobe. Assuming a power-law spectrum of photon index 2 and a column density of 7×10^{20} cm^{-2}, the X-ray luminosity (0.1–10 keV) of the southwest lobe is approximately 9.1×10^{38} ergs s^{-1}.

3.3. *Discrete Point Sources within Cen A*

We applied the wavelet decomposition algorithm for source detection described by Vikhlinin et al. (1995; see also Grebenev et al. 1995 and references therein). This method utilizes approximately Gaussian filters of different scales and hence ap-

proximates an optimal matched filter (e.g., Pratt 1978) for azimuthally symmetric sources. Far off-axis, the algorithm is not optimal, but we have restricted our analysis to a high detection threshold, 5 σ, and have verified by eye that no sources of comparable intensity were undetected and that all detected sources were clearly visible. We used an image binned in 2″ pixels (16 × 16 HRC pixels) and summed the first three wavelet scales (2″, 4″, 8″) to define source existence. The largest of the three scales (8″) is a reasonable size for detecting sources at the edge of the HRC-I field of view. The faintest source detected has 10 source counts (above background), which corresponds to a limiting luminosity of 1.7×10^{37} ergs s^{-1} at the distance of Cen A for a 5 keV bremsstrahlung spectrum and Galactic absorption.

A total of 63 sources were detected as well as an additional 11 sources within or near the jet/counterjet regions which we exclude. Of these 63 sources, 21 were previously detected in *ROSAT* images (Turner et al. 1997; Ruiz, Jones, & Forman 2000). Seven other sources detected by *ROSAT* are not seen in our data. Two *Chandra* sources are more than twice the minimum detectable *ROSAT* flux and should have been detected by *ROSAT* if they had a constant flux. These two sources (CXJ $13^h25^m58\overset{s}{.}8$, −43°04′30″ and CXJ $13^h25^m07\overset{s}{.}7$, −43°01′14″) thus are likely to be highly variable or transient sources. Of the newly detected sources, we detect four that are identified with optically selected globular clusters (Harris et al. 1992; Minniti et al. 1996) (CXJ $13^h25^m54\overset{s}{.}5$, −42°59′24″, CXJ $13^h25^m41\overset{s}{.}5$, −42°59′18″, CXJ $13^h25^m34\overset{s}{.}0$, −42°58′59″, and CXJ $13^h25^m32\overset{s}{.}4$, −42°58′51″). X-ray emission from SN 1986G is not detected in excess of 3×10^{37} ergs s^{-1}. The radial source distribution of the 63 *Chandra* sources demonstrates that most of the sources are associated with Cen A since they are highly concentrated toward the galaxy center. The source density declines monotonically from a peak of 1.9 sources $arcmin^{-2}$ within 1′ to 10% of the peak value in the annulus from 3′ to 5′. Within 5′ of the center, there are a total of 38 sources.

4. SUMMARY AND CONCLUSIONS

We have presented preliminary results of a *CXO*/HRC observation of the radio galaxy Cen A and have demonstrated that the imaging resolution is better than 1″. We also have qualitatively described some detector properties and an event-filtering algorithm that must be applied to HRC data for optimal angular resolution. We have found that the nucleus is extended by a few tenths of an arcsecond (~5 pc) and that each of the knots in the X-ray jet has a complex spatial morphology. Knot-like and extended diffuse emission in the opposite direction of the jet may be an X-ray counterjet. We have also determined that the inner jet may be partially obscured by the dust lane, and confirmed the detection of X-ray emission from the southwest radio lobe. Sixty-three galactic sources were detected, four of which are coincident with globular clusters.

We would like to thank the anonymous referee for comments that improved the Letter. This work was supported by NASA contracts NAS8-38248, NAS8-39073, and NAS8-40224.

REFERENCES

Brodie, J., Konigl, A., & Bowyer, S. 1983, ApJ, 273, 154
Burns, J. O., Feigelson, E. D., & Schreier, E. J. 1983, ApJ, 273, 128
Clarke, D. A., Burns, J. O., & Norman, M. L. 1992, ApJ, 395, 444
Döbereiner, S., et al. 1996, ApJ, 470, L15
Fabian, A. C. 1977, Nature, 269, 672
Feigelson, E. D., Schreier, E. J., Delvaille, J. P., Giacconi, R., Grindlay, J. E., & Lightman, A. P. 1981, ApJ, 251, 31
Giacconi, R., et al. 1979, ApJ, 230, 540
Grebenev, S. A., Forman, W., Jones, C., & Murray, S. 1995, ApJ, 445, 607
Harris, G. L. H., Geisler, D., Harris, H. C., & Hesser, J. E. 1992, AJ, 104, 613
Israel, F. P. 1998, A&A Rev., 8, 237
Jones, D. L., et al. 1996, ApJ, 466, L63
Kenter, A. T., et al. 1997, Proc. SPIE, 3114, 26
Kraft, R. P., et al. 1997, Proc. SPIE, 3114, 53
Marconi, A., Schreier, E. J., Koekemoer, A., Capetti, A., Axon, D., Macchetto, D., & Caon, N. 2000, ApJ, 528, 276
Mauche, C. W., & Gorenstein, P. 1986, ApJ, 302, 371
Minniti, D., Alonso, M. V., Goudfrooij, P., Jablonka, P., & Meylan, G. 1996, ApJ, 467, 221
Morini, M., Anselmo, F., & Molteni, D. 1989, ApJ, 347, 750
Murray, S. S., & Chappell, J. H. 1988, Proc. SPIE, 982, 48
Murray, S. S., Chappell, J. H., Elvis, M. S., Forman, W. R., & Grindlay, J. E. 1987, Astrophys. Lett. Commun., 26, 113
Murray, S. S., et al. 1997, Proc. SPIE, 3114, 11
Pratt, W. K. 1978, Digital Image Processing (New York: Wiley)
Ruiz, T., Jones, C., & Forman, W. 2000, ApJ, submitted
Schiminovich, D., van Gorkom, J. H., van der Hulst, J. M., & Kasow, S. 1994, ApJ, 423, L101
Schreier, E. J., Feigelson, E., Delvaille, J., Giacconi, R., Grindlay, J., Schwartz, D. A., & Fabian, A. C. 1979, ApJ, 234, L39
Schreier, E. J., et al. 1998, ApJ, 499, L143
Turner, T. J., George, I. M., Mushotzky, R. F., & Nandra, K. 1997, ApJ, 475, 118
van den Bergh, S. 1976, ApJ, 208, 673
Vikhlinin, A., Forman, W., Jones, C., & Murray, S. 1995, ApJ, 451, 542
Weisskopf, M. C., O'Dell, S. L., Elsner, R. F., & Van Speybroeck, L. P. 1995, Proc. SPIE, 2515, 312
Zombeck, M. V., David, L. P., Harnden, F. R., & Kearns, K. 1995, Proc. SPIE, 2518, 304